師大地理研究報告
第35期　民國90年11月
Geographical Research
No. 35, November. 2001

EJ095200135121

結合空載超光譜和雷達資料增揚都市地表特徵

The Integration of Hyperspectral and Radar data to Enhance Urban Surface Features

陳哲銘*
Che-Ming Chen

Abstract

Due to the complexity of urban surface materials, it is inefficient to discriminate urban land covers by a single sensor. In this project, the Intensity-Hue-Saturation (IHS) transformation is used to integrate the high spectral resolution, provided by the hyperspectral data (AVIRIS), and the surface texture information, derived from radar data (TOPSAR), into a single image. The spectral ambiguity of several urban land covers is resolved in the merged image with higher spectral and spatial resolution. This image is also superimposed on the DEM data derived from TOPSAR data to create a 3-D perspective view. For the urban areas where are at risk of geological hazards (e.g., mudflows and debris flows), the 3-D perspective view of the fused image can be applied to simulate the movement of mudflows and predict the areas and buildings at risk.

Keywords: Intensity-Hue-Saturation transformation、data fusion、hyperspectral data、radar data、3-D perspective view

* 國立台灣師範大學地理系副教授

中文摘要

都市地物的種類多樣，透過單一感測器的資料往往無法有效判別地物特徵，本研究利用「明暗-色相-飽和度轉換法」(Intensity-Hue-Saturation transformation)來融合空載超光譜(AVIRIS)和雷達(TOPSAR)影像，以整合超光譜影像所提供的高光譜解析力和雷達影像所提供的地表組織與粗糙度等資訊於單一的影像中，並將此整合的影像疊合TOPSAR所提供的數值地形模型(DEM)資料，產生三維立體影像。對臨近山坡地的都市地區，此方法所產生的三維立體影像，由於同時具有地物和地形特徵，未來可被應用於模擬泥流或土石流災害。

關鍵詞：明暗-色相-飽和度轉換法、影像融合、超光譜影像、雷達影像、三維立體影像

Introduction

The data fusion of multisensor data has received tremendous attention in the remote sensing literature (Yao and Gilbert, 1984; Welch and Ehlers, 1988; Chavez *et al.*, 1991; Weydahl *et al.*, 1995; Niemann *et al.*, 1998; Saraf, 1999; Zhang, 1999). Recently, NASA's Jet Propulsion Laboratory merged three datasets to create a 3-D perspective view of Pasadena area, California in which the Shuttle Radar Topography Mission (SRTM) supplied the elevation data, Landsat TM provided the land surface color, and USGS digital aerial photography supplied the image details. The resultant image demonstrated that the advantages of the spatial detail, the spectral detail, and the topographical detail derived from different sources could be maximized by a data fusion technique (NASA, 2000).

Since many land covers / surface materials spectrally and spatially mix together within a pixel in an urban scene, it's difficult to analyze the urban scene with a single sensor (Hepner *et al.*, 1998). For example, some land cover types are spectrally indistinguishable from each other within a Landsat TM scene, such as asphalt vs. water or shadow, trees and shrubs vs. lawns, and bare soil vs. newly completed concrete sections (Wheeler, 1985). On the other hand, many different cover types, for example, tiled roofing materials, asphalt, concrete, grass, trees, soil and water, often mixed within a pixel in the scene of urban residential areas. Radiation from a single pixel on the ground may therefore be derived from a number of surfaces, and each has its own distinct spectral signature giving an additive response. Consequently,

an image pixel is not representative of any one land-cover type on the ground (Forster, 1985).

The data fusion technique is capable of integrating different data, and more information can be obtained than that derived from a single sensor data. Particularly, the geophysical information extracted from the optical and microwave wavelengths has been proved useful to characterize mineralogy and morphology of surfaces (Kierein-Young, 1997). The former measured the surface-radiation interactions at the molecular scale giving information about the mineralogical makeup of the surface. The latter recorded the transmitted radiation scattered from the surface textural and dielectric variations providing information about the morphology and moisture content of the surface. The integrated image, therefore, provided the complementary information and improved the understanding of the variability in surfaces. This approach should also be feasible for extracting more urban surface features from multisensor data. For example, the spectral confusion of bare soil and concrete roofs in a VIR urban scene could be resolved by a radar image in which buildings have relatively high amplitude due to corner reflector, and bare soil has relatively low amplitude resulted from specular reflector. On the other hand, both trees and buildings have high amplitude so that they are confused with each other in a radar image. However, this confusion could be easily resolved by a broadband VIR image.

The objective of this study is to demonstrate a rapid and effective approach for merging AVIRIS and TOPSAR data. An image-enhancement technique, Intensity-Hue-Saturation (IHS) transformation, is adopted to conduct the data fusion. The fused image is expected to provide a new component with high spatial resolution, high spectral resolution, and elevation information. For the urban areas where are at risk of geological hazards (e.g., mudflows and debris flows), such an image can be applied to simulate how mudflows or debris flows will be channeled down the canyons

Study Area

The urban area of Park City, Utah (Figure. 1) was chosen as the study area due to the representative of mixture of land covers for western U.S. cities and other urban areas of the earth undergoing rapid urban growth. It also provides a typical example where urbanization spreads from lowlands to adjacent uplands. Although Park City

area is not highly urbanized, it contains the diversity of land covers, surface materials, and vegetation associations that can be found in many western U.S. cities. Therefore, the data fusion approach investigated in this study should be transferable to the other western U.S. cities.

Data Acquisition

TOPSAR data

The TOPSAR data used in this study refer to the AIRSAR data acquired in the in the TOPSAR XTI1 mode which generated a C-band Digital Elevation Model (DEM) along with L- and P-band polarimetry. The integrated TOPSAR data product consisted of a number of different data types such as DEM, C-Band VV data, incidence angle map, correlation map, L-Band Polarimetry data, and P-Band Polarimetry data.

All data files are in ground range projection and in range line format in which each record in the data file corresponds to constant along-track position (azimuth) and varying cross-track position (range). The ground data projection was conducted using the DEM data derived from the C-band interferometry. The DEM data represent the elevation of the terrain above a spherical approximation to the WGS-84 ellipsoid with a 10-m pixel size.

The TOPSAR data over Park City area were collected on October 28, 1998. The P-band data were collected at 20MHz bandwidth while the C-band and L-band data were collected at 40MHz. The resultant P-band data are in the slant range and are not co-registered with the other two frequencies due to the difference in bandwidth.

AVIRIS data

Airborne Visible Infrared Imaging Spectrometer (AVIRIS) is an optical sensor that delivers calibrated images of the upwelling spectral radiance in 224 contiguous spectral bands with wavelengths from 400 to 2500 nm. The high-altitude AVIRIS data of Park City area were obtained on 5 August 1998. The data range for this imagery is from Band 1, with a bandcenter of 369.07 nm, to Band 224, with a bandcenter of 2507.50. The AVIRIS radiance data of the study site were calibrated to reflectance data using a radiative transfer model (ATREM) and *in situ* spectra from several calibration sites.

Ground Truth Data

The USGS 1:24000 scale Digital Orthoquad (DOQ) maps of Park City area were used to provide ground control points and to geometrically rectify the TOPSAR and AVIRIS images. Since the DOQ maps were obtained in 1993 whereas the AVIRIS and the TOPSAR data were acquired in 1998, many land covers were changed in the study area. Field checks were conducted to provide the complementary ground truth data.

Techniques for Data Fusion

Minimum Noise Fraction (MNF) Transformation

There are 224 bands in the AVIRIS data. However, only 3 bands can be used to perform the IHS transformation. Besides, the spectral bands exhibit rather high interband correlations, and a large amount of redundancy exists among the spectral images. Therefore, the MNF transformation was used to reduce the data dimensionality of AVIRIS data before performing the data fusion.

The MNF transformation was first developed to investigate the improvement by comparing the MNF transformation with the principal components analysis in airborne thematic mapper (ATM) ten-band data (Green *et al.*, 1988). The MNF transformation was defined as two cascaded principal components transformation. The first step, based on an estimated noise covariance matrix, is to decorrelate and rescale the noise in data where the noise has unit variance and no band-to-band correlations. The next step is a standard principal components transformation of the noise-whitened data.

The MNF transformation was derived as an analogue of the principal components transformation and has all the properties of the principal components transformation, including the primary characteristic of optimally concentrating the information content of the data in as small a number of components as possible (Lee *et al.*, 1990). It is invariant under scale changes to any band since it depends on signal-to-noise ratios. This transformation is equivalent to principal components when the noise variance is the same in all bands and it reduces to a multiple linear regression when noise is in one band only (Green *et al.*, 1988). By applying the MNF to the Geophysical and Environment Research (GER) 64-band data, the results demonstrated the effectiveness of this transformation for noise removal in both the

spatial and spectral domains (Lee *et al.*, 1990).

The MNF transformation was chosen because it not only could reduce the data dimension but also order components in terms of image quality, the signal-noise ratio (SNR). The special capability of the MNF, which shows steadily decreasing image quality with increasing component number, may not be accomplished by other techniques such as principal components analysis and factor analysis (Green *et al.*, 1988; Lee *et al.*, 1990; Chen, 2000).

Intensity-Hue-Saturation (IHS) Color Transformation

IHS is one of the most often used methods to merge multisensor image data. It was first used to merge Landsat MSS with Return Beam Vidicon (RBV) data and Landsat MSS with Heat Capacity Mapping Mission data (Haydn *et al.*, 1982). The method uses three bands of the lower spatial resolution data set and transforms these data into IHS space. A contrast stretch has been applied to the higher spatial resolution image so that the stretched image has approximately the same variance and average as the intensity component image. Then, the stretched, higher resolution image replaces the intensity component before the image is transformed back into the original space (Chavez *et al.*, 1991).

The IHS color coordinate system is based on a hypothetical color sphere. The vertical axis represents intensity, which ranges from 0 (black) to 255 (white). The circumference of the sphere represents hue, which is the dominant wavelength of color. Hue ranges from 0 at the midpoint of red tones to 255 adjacent to 0. Saturation represents the purity of the color and ranges from 0 at the center of the color sphere to 255 at the circumference (Jensen, 1996). The IHS values could be derived from the RGB values through transformation equations. The following equations were used to compute IHS values for a SPOT data set with 3 bands of data (BV_1, BV_2 and BV_3). The IHS values could also be converted back into RGB values using the inverse of these equations (Pellemans *et al.*, 1993):

$$I = (BV_1 + BV_2 + BV_3) / 3$$

$$H = [\arctan (2\,BV_1 - BV_2 - BV_3) / \sqrt{3}\,(BV_2 - BV_3)] + C$$

Where $C = 0$, if $BV_2 \geq BV_3$; $C = \pi$, if $BV_2 < BV_3$

$$S = \sqrt{6}\,(BV_1^2 + BV_2^2 + BV_3^2 - BV_1\,BV_2 - BV_1\,BV_3 - BV2\,BV_3)^{-0.5} / 3$$

The IHS transformation has been used to merge SIR-B and Landsat TM images (Welch and Ehlers, 1988). It was found that the completeness cartographic features extracted from the composite SIR-B/TM image exceed those obtained from individual TM and SIR-B images by approximately 10 and 25 percent, respectively.

Image Processing

Image Georectification

The USGS 1:24000 scale DOQ maps were used as the reference images. The study area is covered by two map sheets, West Park City and East Park City. These images were mosaicked to create a single map. Since the 1998 AVIRIS flight line over the study area was from south to north, the AVIRIS image was first rotated 180 degree to match the orientation of the DOQ maps. The image-to-map rectification process was used to register the AVIRIS image to the reference map. Fifteen ground control points (GCPs) were selected in the image along with their corresponding map coordinates. The polynomial 1st order and the nearest neighbor were chosen as the wraping and resampling methods. The output projection for the registered image was UTM zone 12 with NAD83 datum and the AVIRIS image was resampled to 10m pixel size. The total RMS error is 0.76 pixel.

Similar geometric corrections were applied to the TOPSAR data (Figure. 2). The images of the L-band 4 channels and DEM data were rotated 270 degree with the same orientation as the reference map. Fifteen ground control points (GCPs) were located. It is more difficult to accurately identify GCPs in the TOPSAR image than in the AVIRIS image. Thus, the RMS error of the TOPSAR rectification is 1.195 pixels, which is higher than that of the AVIRIS data. While the pixel size of TOPSAR image is 10m and the AVIRIS image is 20m, the geometric quality of the rectified AVIRIS and TOPSAR data is approximately at the same level.

Imaging Processing for the Data Fusion

As the goal of this study is to merge the AVIRIS data and the TOPSAR data with DEM, the following procedures are applied. The MNF transformation was performed to reduce the dimensionality of the AVIRIS data. Only three bands, which are consisted of more urban surface features than the other bands in the

MNF-transformed image, were chosen as the input of the IHS transformation. The brightness range of the AVIRIS data was converted from 16 bits to 8 bits to match the range of the hue in the IHS color system. The three bands of the converted AVIRIS image were assigned to color red (R), green (G), and blue (B) and then converted into the IHS color system. By comparing the L-band HH, VV, and HV-polarized images, the HV image appears to be better than the other images for detecting the urban surface features. Thus, the L-band HV TOPSAR image was chosen as the high spatial resolution image to replace the intensity of the IHS-transformed AVIRIS image. The number of looks processed in azimuth was retained at 36 to prevent the further degradation of the spatial detail in the TOPSAR L-band HV image. A contrast stretch algorithm using square root was applied to the L-band HV image to take advantage of the full data range (0 to 255), and the contrast of this image was, therefore, enhanced. The intensity component of the AVIRIS image was replaced by the contrast-stretched TOPSAR L-band HV image. The IHS-transformed image was converted back into RGB color space. The merged image was superimposed on the DEM data to create a 3-D perspective view of the study area.

Results

As expected, MNF successfully ordered components in terms of image quality (Figure 3). There is a definite trend to increasing noise with increasing component number (Table. 1). The grass/crop vegetation has relatively higher brightness than that of built-up areas in the first component. The grassland (golf course) in the upper portion of the second component was apparently identifiable due to very high brightness, and the water bodies of ponds in the golf courses were relatively very dark. The bare soil of ski trails and mining tailings was revealed in the third component with very high brightness. Among the first 9 components, components 1, 2, and 3 spectrally revealed most of the surface features so that they were chosen to be

Table. 1 Eigenvalues of the first 9 MNF components

Component	1	2	3	4	5	6	7	8	9
Eigenvalue	4099.65	3166.15	2318.12	1438.02	758.28	544.74	371.07	315.59	198.42

converted into the IHS color space. The first component was assigned to green color, the third component, blue, and the second component, red (Figure. 4). Through comparison with the DOQ map, it was found that the magenta color indicated buildings, roads, and mining tailings. The cyan color revealed mature woodlands. The yellow color depicted grass and crops. The blue color indicated bare soil. The green spots surrounded by yellow color were water bodies (ponds). The north sides of mountains were in shadow depicted by green color in the lower portion of the image.

In the contrast-stretched, L-band HV TOPSAR image (Figure. 5), "very bright" areas included buildings and mature woodlands; "very dark" areas included ski trails, roads, and grasslands (ranches and golf courses). It's difficult to separate these surface features based on the brightness because the different land covers described above have the similar brightness. However, several of them could be separated by the different surface roughness and texture. For example, the downtown areas looked very speckled but the woodlands looked relatively smoother. If ground truth information or previous knowledge about the study area were not available, the highways would not be apparently separable from the ski trails because both of them have the similar brightness, roughness, and texture.

Compared to the originally MNF-transformed AVIRIS image, the spatial resolution of the AVIRIS/TOPSAR merged image was significantly enhanced by the L-band HV TOPSAR image (Figure 6). For example, the linear features such as roads and ski trails were much more identifiable than those in the original AVIRIS image. The merged image also revealed surface roughness which was not presented in the AVIRIS image. Originally, the buildings and mining tailings were spectrally undistinguishable in the MNF-transformed AVIRIS image because both of them were indicated by the same color, blue. In the merged image, the former has very high reflectance (brighter) and the latter has very low reflectance (darker). On the other hand, the originally L-band HV TOPSAR image was spectrally enhanced by the AVIRIS image. For example, both pine trees and buildings have very high amplitude in the L-band HV TOPSAR image. However, they were separated by the different colors in the merged image. The former was indicated by cyan color and green color (in shadow), as the latter was presented by magenta color.

It should be noted that the spectral resolution of the AVIRIS MNF image was partially degraded by the L-band HV TOPSAR image. Several surface features (e.g., ski trails, fairways of the golf courses, and lawns of the softball field and the city cemetery) have relatively low amplitude resulted from specular reflector. When the intensity of the AVIRIS MNF image was replaced by the L-band HV TOPSAR image and converted back to the RGB space, these surface features were too dark to differentiate from each other.

A 3-D perspective view generated by superimposing the AVIRIS/TOPSAR merged image on the DEM (Figure 7). No vertical exaggeration was applied on this image. The Park City ski area was showed on the right portion of the image. The downtown area of Park City was presented in the middle as a magenta belt. The dominant vegetation community, mountain brush, was found at lower elevations around the left side of the Park City downtown area and indicated by gray color. The pine trees were also found within the study area at higher elevations and presented by cyan and green color. The confusion between roads and ski trails in the L-band HV TOPSAR image was resolved by the topography and the spatial pattern in the perspective view.

Conclusions

In this study, the merged image and its 3-D perspective view demonstrate that the IHS transformation is capable of integrating AVIRIS and TOPSAR images. Urban surface features were more distinguishable from each other by using the AVIRIS/TOPSAR merged image than by using a single sensor data. The spatial resolution derived from the L-band HV TOPSAR image successfully enhanced the AVIRIS image. On the other hand, the spectral resolution derived from the MNF-transformed AVIRIS image also improved the discriminability of the L-band HV TOPSAR image. As expected, the spectral confusion between buildings and mining tailings in the AVIRIS image were resolved by the different amplitude presented by the TOPSAR L-band HV image. The confusion between trees and buildings due to the high amplitude in the radar image was resolved by the different colors generated by the MNF-transformed AVIRIS image. Moreover, the 3-D perspective view revealed the topographic and textural information which resolved the confusion between the ski trails and highways in the TOPSAR image.

The major source of color distortion in the merged image was contributed by the limited gray scale of the TOPSAR L-band HV image. Several surface features such as fairways of golf courses and ski trails were not differentiable in the TOPSAR image due to the low reflectance close to 0. The low intensity would result in the low RGB values of these features in the merged image. Consequently, the color (i.e., spectral resolution) of these features was lost.

The procedure of conducting the MNF transformation, IHS transformation and DEM overlay also provides a rapid, easy, and effective approach for creating a 3-D perspective scene of the study area. This 3-D perspective scene with urban surface features and topographical features could be applied to simulate the downslope movement of mudflows as well as to estimate the damaged area for future research.

References

Chavez, P. S., S. C. Sides, and J. A. Anderson (1991): Comparison of three different methods to merge multiresolution and multispectral data: Landsat TM and SPOT Panchromatic, *Photogrammetric Engineering & Remote Sensing*, 57(3): 295-303.

Chen, Che-Ming (2000): Comparison of principal components analysis and minimum noise fraction transformation for reducing the dimensionality of hyperspectral imagery, *Geographical Research*, 33:163-178.

Forster, B. C. (1985): An examination of some problems and solutions in monitoring urban areas from satellite platforms, *International Journal of Remote Sensing*, 6(1): 139-151.

Green, A. A., M. Berman, P. Switzer, and M. D. Craig (1988): A transformation for ordering multispectral data in terms of image quality with implications for noise removal, *IEEE Transactions on Geoscience and Remote Sensing*, 26(1): 65-74.

Haydn, R., G. W. Dalke, J. Henkel, and J. E. Bare (1982): Application of the IHS color transform to the processing of multisensor data and image enhancement, *Proceedings of the International Symposium on Remote Sensing of Arid and Semi-Arid Lands*, Cairo, Egypt, pp. 599-616.

Hepner, G. F., B. Houshmand, I. Kulikov, and N. Bryant (1998): Investigation of the Integration of AVIRIS and IFSAR for urban analysis, *Photogrammetric Engineering & Remote Sensing*, 64(8): 813-820.

Jensen, J. R. (1996): Merging different types of remotely sensed data for effective visual display, Introductory Digital Image Processing: A Remote Sensing Perspective, 2nd ed., Prentice-Hall, Upper Saddle River, NJ, pp. 100-103.

Kierein-Young, K. S. (1997): The integration of optical and radar data to characterize mineralogy and morphology of surfaces in Death Valley, California, U.S.A., *INT. J. Remote Sensing*, 18(7): 1517-1541.

Lee, J. B., A. S. Woodyatt, and M. Berman (1990): Enhancement of high spectral resolution remote sensing data by a noise-adjusted principal components transform, *IEEE Transactions on Geoscience and Remote Sensing*, 28(3): 295-304.

Murphy, D. R. (1981): Vegetation zones, *Atlas of Utah*, Brigham Young University, Provo, Utah, pp. 31-32.

NASA (2000): SRTM Web Page, retrieved from http://www.jpl.nasa.gov/srtm

Niemann, K. O., D. G. Goodenough, D. Marceau, and G. Hay (1998): A practical alternative for fusion of hyperspectral data with high resolution imagery, *IEEE International Geoscience and Remote Sensing Symposium*, 1: 174-176.

Pellemans, A. H., R. W. Jordans, and R. Allewijn (1993) Merging multispectral and panchromatic SPOT images with respect to the radiometric properties of the sensor, *Photogrammetric Engineering & Remote Sensing*, 59(1): 81-87.

Saraf, A. K. (1999): IRS-1C-LISS-III and PAN data fusion: an approach to improve remote sensing based mapping techniques, *INT. J. Remote Sensing*, 20(10): 1929-1934.

Welch, R., and M. Ehlers (1988): Cartographic feature extraction with integrated SIR-B and Landsat TM images, *INT. J. Remote Sensing*, 9(5): 873-889.

Weydahl, D. J., X. Becquey, and T. Tollefsen (1995): Combining ERS-1 SAR with optical satellite data over urban areas, *IEEE International Geoscience and Remote Sensing Symposium*, 3: 2161-2163.

Wheeler, D. J. (1985): Evaluation of thematic mapper data for determining urban land cover, Ph.D. dissertation, *University of Utah, Department of Geography*, Salt Lake City, Utah.

Yao, S. S., and J. R. Gilbert (1984): Registration of a synthetic aperture radar image to thematic mapper imagery for remote sensing applications, *IEEE Transactions on*

Geoscience and Remote Sensing, GE-22(6): 557-563.

Zhang, Y. (1999): A new merging method and its spectral and spatial effects, *INT. J. Remote Sensing*, 20(10): 2003-2014.

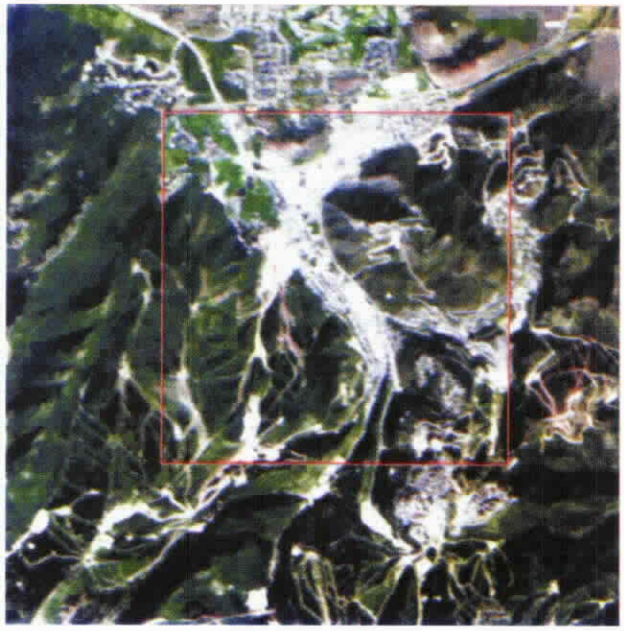

Figure 1. The true-color AVIRIS scene of Park City, Utah, U.S. The red box indicates the area to be merged with TOPSAR data

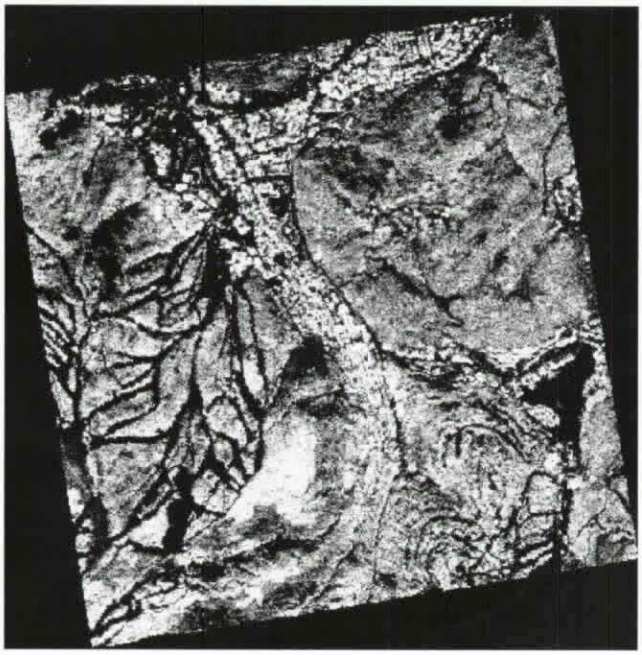

Figure. 2 The rotated and georectified TOPSAR L-band HV image of the study area

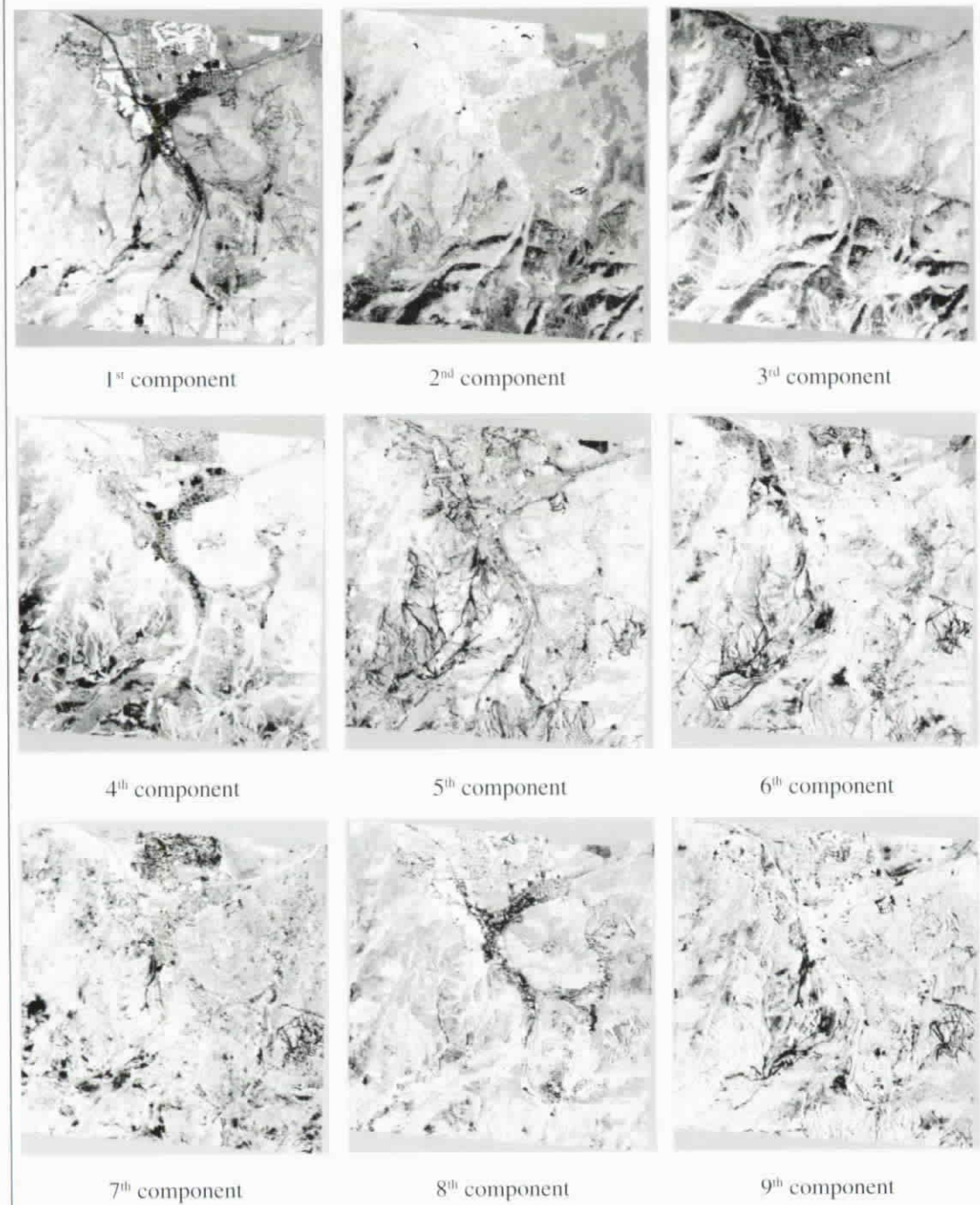

Figure 3. The first 9 components of the MNF-transformed AVIRIS image

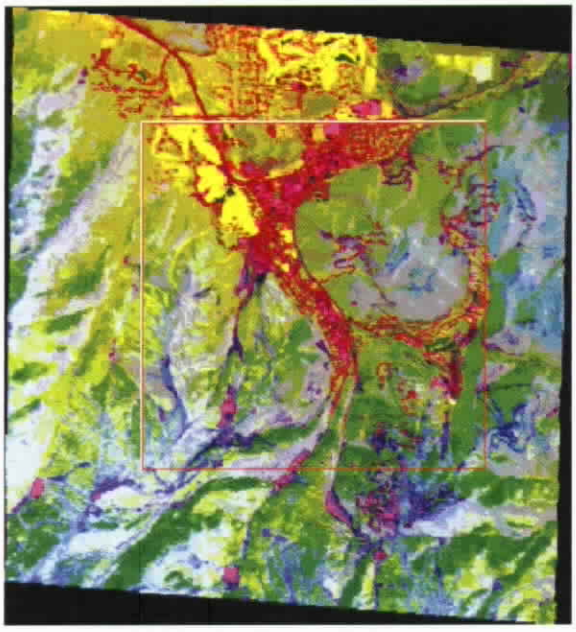

Figure 4. The color composite image of the MNF components 2 (R), 1 (G), and 3(B). The red box indicates the area to be merged with TOPSAR data

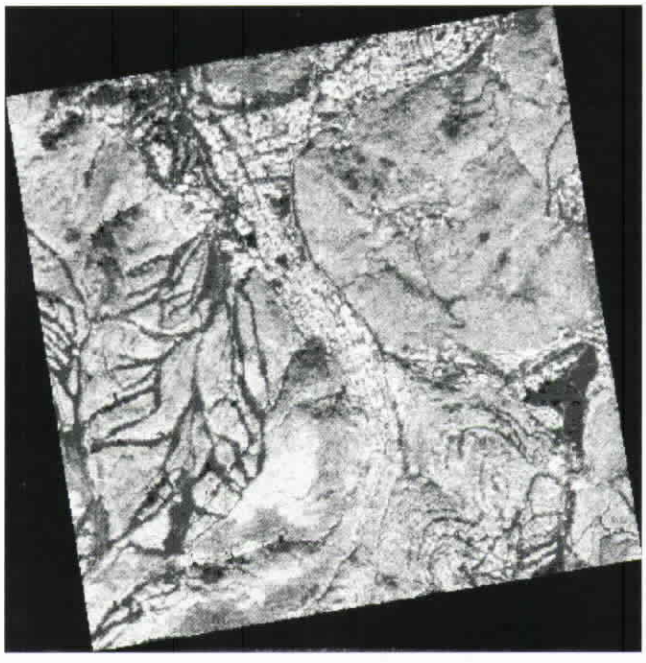

Figure 5. The contrast-stretched, L-band HV TOPSAR image

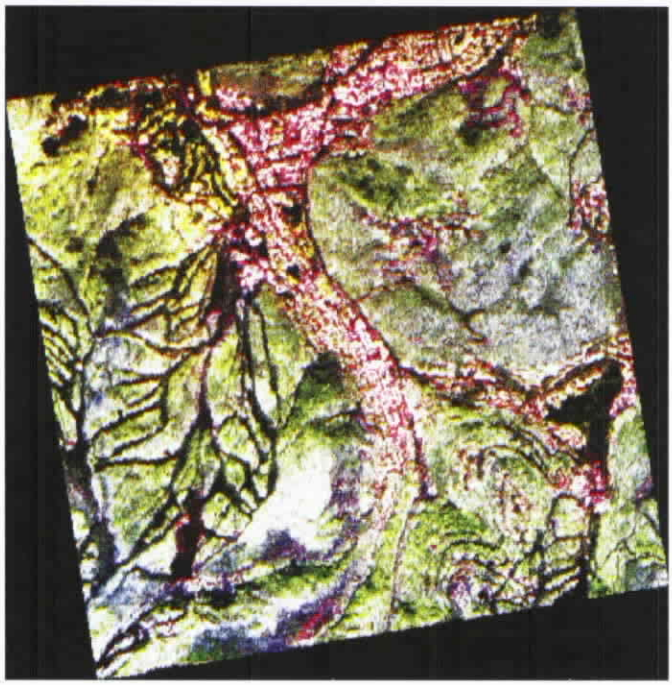

Figure 6. The merged image of the MNF-transformed AVIRIS scene and the TOPSAR L-band HV scene

Figure 7. The 3-D perspective view of the study area (180 ° rotated)

收稿日期：90 年 9 月 30 日
修正日期：90 年 10 月 30 日
接受日期：90 年 11 月 5 日